Article

Acute Central Serous Chorioretinopathy Subtypes as Assessed by Multimodal Imaging

Alessandro Arrigo[1], Emanuela Aragona[1], Alessandro Bordato[1], Alessandro Calamuneri[2], Alessio Grazioli Moretti[1], Stefano Mercuri[1], Francesco Bandello[1], and Maurizio Battaglia Parodi[1]

[1] Department of Ophthalmology, IRCCS Ospedale San Raffaele, University Vita-Salute, Milan, Italy
[2] IRCCS Bonino-Pulejo Neurolesi, Messina, Italy

Purpose: To differentiate acute central serous chorioretinopathy (CSC) subtypes by multimodal imaging.

Methods: The research was designed as a prospective, interventional study. Naive patients with acute CSC were followed for 24 months. Overall, 96 CSC patients (96 eyes) and 210 controls (210 eyes) were included. Multimodal imaging allowed the study to classify CSC into retinal pigment epithelium-related CSC (RPE-CSC) and choroidal-related CSC (choroidal-CSC) subtypes. The RPE-CSC type was characterized by normal choroidal thickness (CT) in association with disseminated RPE alterations. The choroidal-CSC type was distinguished by identifying a pachychoroid. All the patients underwent eplerenone or verteporfin photodynamic therapy (PDT). Patients developing macular neovascularization (MNV) underwent anti-VEGF injections. Quantitative measurements included central macular thickness (CMT), choroidal thickness (CT), Sattler layer thickness (SLT) and Haller layer thickness (HLT).

Results: Considering the CSC patients as a whole, baseline BCVA was 0.18 ± 0.25 LogMAR, increasing to 0.13 ± 0.21 LogMAR after 24 months ($P < 0.01$), whereas baseline CMT improved from 337 ± 126 μm to 244 ± 84 μm after 24 months ($P < 0.01$). We found the following subdivision of CSC eyes: RPE-CSC type (45%) and choroidal-CSC type (55%). Overall, MNV were detected in 18 eyes (19%), 13 eyes (72%) in the RPE-CSC subgroup and five eyes (28%) in the choroidal-CSC subgroup.
Forty eyes responded to eplerenone (57% of RPE-CSC and 47% of choroidal-CSC), whereas 38 eyes required PDT (43% of RPE-CSC and 53% of choroidal-CSC).

Conclusions: Acute CSC includes two main clinical manifestations, displaying differing features concerning retinal and choroidal involvement.

Translational Relevance: This study identified two clinically different acute CSC subtypes on the basis of quantitative pachychoroid cutoff values.

Introduction

The pathogenesis of central serous chorioretinopathy (CSC) is multifaceted and still poorly understood.[1–3] Traditionally, CSC has been related both to choroidal abnormalities and to retinal pigment epithelium (RPE) dysfunction.[3] CSC can be clinically subdivided into acute and chronic forms, according to the duration of the disease and the extent of the posterior pole involvement.[1,2] A predisposing factor associated with the risk of CSC onset is the presence of pachychoroid. Indeed, the abnormal size of choroidal vessels has been strongly associated with the onset and progression of subretinal fluid, characterizing CSC.[1,2] However, pachychoroid cannot be considered as a pathognomonic factor of CSC, because pachychoroid can be also associated with other macular disorders and because CSC may occur in the case of a normally appearing choroid. Further-

1

more, to date, a precise definition of pachychoroid with specific cutoff values to identify these abnormal vessels is still lacking. Furthermore, we still lack a precise classification stemming from the pathogenesis of the disease. A pathogenic categorization would be useful in selecting the most appropriate treatment to improve anatomic and functional outcomes. Fortunately, the introduction of multimodal imaging, including optical coherence tomography (OCT) and optical coherence tomography angiography (OCTA), has offered new tools in the quest to expand our understanding of CSC.

The aim of the present study was to analyze multimodal imaging findings involving naive patients affected by acute CSC, to identify different disease subtypes and correlate them with the outcome achieved after two years of follow-up. A secondary goal will be the identification of a possible CSC phenotype associated with an increased risk of onset of neovascular complication.

Methods

The study was designed as a prospective, interventional case series with a 24-month follow-up. One hundred and eighteen eyes of 118 patients presenting naive CSC at the first clinical episode, showing visual acuity decline and/or metamorphopsia with under three-month duration, were recruited at the Ophthalmology Unit of San Raffaele Hospital, Milan, Italy, between January 2015 and October 2016. Signed informed consent was obtained from all patients. The study was conducted in accordance with the Declaration of Helsinki and was approved by the Ethical Committee of the Vita-Salute San Raffaele University in Milan.

The diagnosis of CSC was made through fundus autofluorescence (FAF), structural optical coherence tomography (OCT), fluorescein angiography (FA), and indocyanine green angiography (ICGA) images (Spectralis HRA+OCT; Heidelberg Engineering, Heidelberg, Germany). The diagnosis was confirmed through the detection of subretinal fluid on structural OCT, corresponding to leakage on FA and choroidal hyperpermeability on ICGA.

The following exclusion criteria were considered: refractive error over ±3D, media opacities, any other type of retinal or optic nerve diseases (assessed through an accurate clinical history analysis and differential diagnosis with other retinal diseases), ocular surgery within the last six months, previous use of steroids, any other systemic conditions, including uncontrolled arterial hypertension, uncontrolled diabetes mellitus, endocrine system disorders, and genetic disorders.

Ophthalmological examination included best corrected visual acuity (BCVA) measurement by standard Early Treatment for Diabetic Retinopathy Study (ETDRS) charts, slit lamp biomicroscopy of anterior and posterior segments, and Goldmann applanation tonometry. The structural OCT acquisition protocol included raster, radial, and dense scans with a high number of frames (automatic real time >50) and enhanced depth imaging (EDI). Structural OCT scans were used to measure central macular thickness (CMT) and retinal thickness (RT) at baseline and over the entire follow-up. These measurements were obtained by raster structural OCT, using the ETDRS thickness map provided by Heidelberg software. In particular, CMT represented the value of the central ring of the ETDRS grid, whereas RT was obtained from the mean value of all the sectors of the same grid. We also used raster structural OCT to evaluate outer retinal alterations (including pigment epithelium detachment (PED), hyperreflective debris, and RPE band signal attenuation over the entire posterior pole.

All patients underwent a treatment strategy scheduling eplerenone (25 mg the first week followed by 50 mg thereafter) as first-line treatment, administered soon after the baseline examination. Patients not responsive to eplerenone were switched to half-dose verteporfin photodynamic therapy (PDT). In the case of plerenone, treatment response was judged to depend on the persistence of at least 250 µm of fluid after three months of treatment, whereas for PDT it hinged on identifying the same amount of fluid three months after the treatment. This thickness was measured measuring the point of maximal fluid thickness on the horizontal structural OCT scan, centered on the fovea. CSC patients with macular neovascularization (MNV) were treated with an initial ranibizumab injection, followed by a pro re nata treatment regimen, which was adopted if any fluid was identified on structural OCT.

We collected an adequate sample of healthy age- and sex-matched eyes (210 eyes of 210 patients; refractive error <±3D), examined by structural OCT, to provide valid reference cutoff values for the definition of pachychoroid.

In case of bilateral CSC, the study eye was randomly selected according to random number generation. With respect to the healthy controls, we randomly considered a single eye for the measurements according to random number generation.

We measured choroidal thickness (CT), and both Sattler and Haller layer thickness (SLT and HLT,
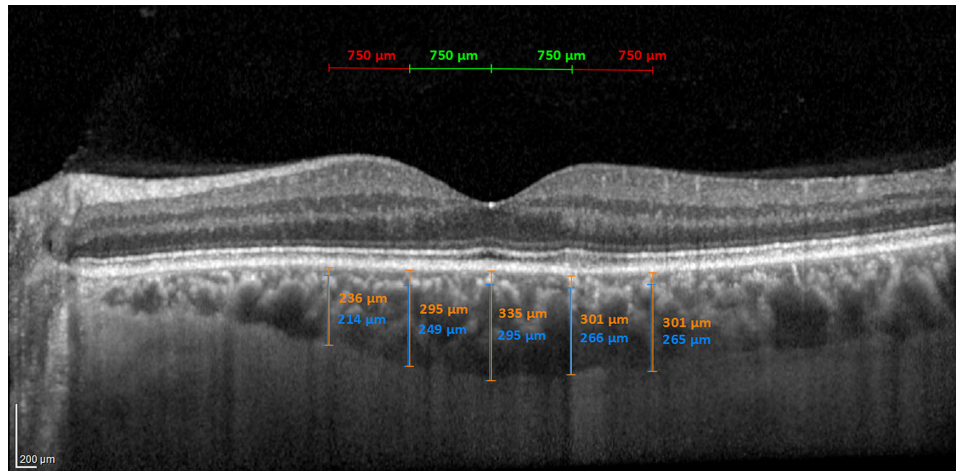
Figure 1. Schematic representation of the quantitative choroidal measurements. CT (*orange*) and HLT (*blue*) measures are performed on a horizontal line, passing through the fovea. The final values are obtained calculating the average of five different measurements: subfoveal, 750 μm (temporal and nasal) and 1500 μm (temporal and nasal). SLT is calculated by subtracting HLT from CT for all measures; the mean value is considered as the final SLT.

respectively). The thickness of the middle choroidal vessel layer (Sattler layer) and the choriocapillaris layer was calculated by subtracting the thickness of the large choroidal vessel layer (Haller layer) from the total choroidal thickness. All the measurements were performed by two experienced examiners (EA and AB) and the mean measurement was used for the purpose of the analysis. The final value represented the average of five different measurements performed on a horizontal EDI structural OCT scan passing through the fovea: subfoveal, 750 μm (temporal and nasal) and 1500 μm (temporal and nasal) (Fig. 1). The same expert graders performed all the measurements at least twice to gauge reproducibility and repeatability. We also calculated the interclass correlation coefficient (ICC) to assess inter-grader agreement through a two-way random-effects model, giving a value of 0.95 (range 0.93–0.98; $P < 0.001$). Overall reproducibility and repeatability were 0.97 and 0.96 for CT; 0.96 and 0.95 for HLT; 0.94 and 0.90 for SLT (all $P < 0.001$).

We identified a quantitative cutoff based on healthy values, which we used to define a pachychoroid. We considered our CSC eyes to display a pachychoroid when the CT value was greater than CT + 2 STD, as measured in healthy controls. After dividing patients according to this cutoff value, we statistically evaluated possible differences in terms of visual and anatomical outcomes.

In this way we subdivided CSC into RPE-related CSC (RPE-CSC), when prevalent RPE impairment was detected in the absence of choroidal thickening, or choroidal-related CSC (choroidal-CSC), when a pachychoroid was identified.

The main outcome of the study was to characterize the different CSC subtypes on the basis of the combined data provided by the multimodal imaging of naive patients affected by acute CSC. Secondary outcomes included the correlations between CSC subtypes, and final anatomic and functional outcomes.

The statistical analyses were performed using SPSS software (SPSS, Chicago, IL). We tested the statistical differences in terms of baseline and final BCVA and CMT values between CSC versus healthy eyes by means of the unpaired *t*-test, setting the statistical significance at $P < 0.05$. The statistical comparison between all the follow-up visits was performed through repeated ANOVA measurement. We also used a one-way ANOVA analysis to carry out the statistical assessment of RPE-CSC versus choroidal-CSC versus healthy controls. In this case, in view of the multiple testing, we adopted the Bonferroni approach to accommodate the numerous comparisons; this procedure gave rise to an alpha value of $0.05/12 = 0.004$, which was required to obtain an overall alpha value of 0.05.

Results

We recruited 118 eyes of 118 patients affected by acute, first-episode CSC. Twenty-two eyes were excluded for the following reasons: high media opacities (18) and glaucoma (4). Overall, 96 eyes of 96 CSC patients (mean age 53 ± 12 years; 80 males (83%)) were included in the analyses and were compared with
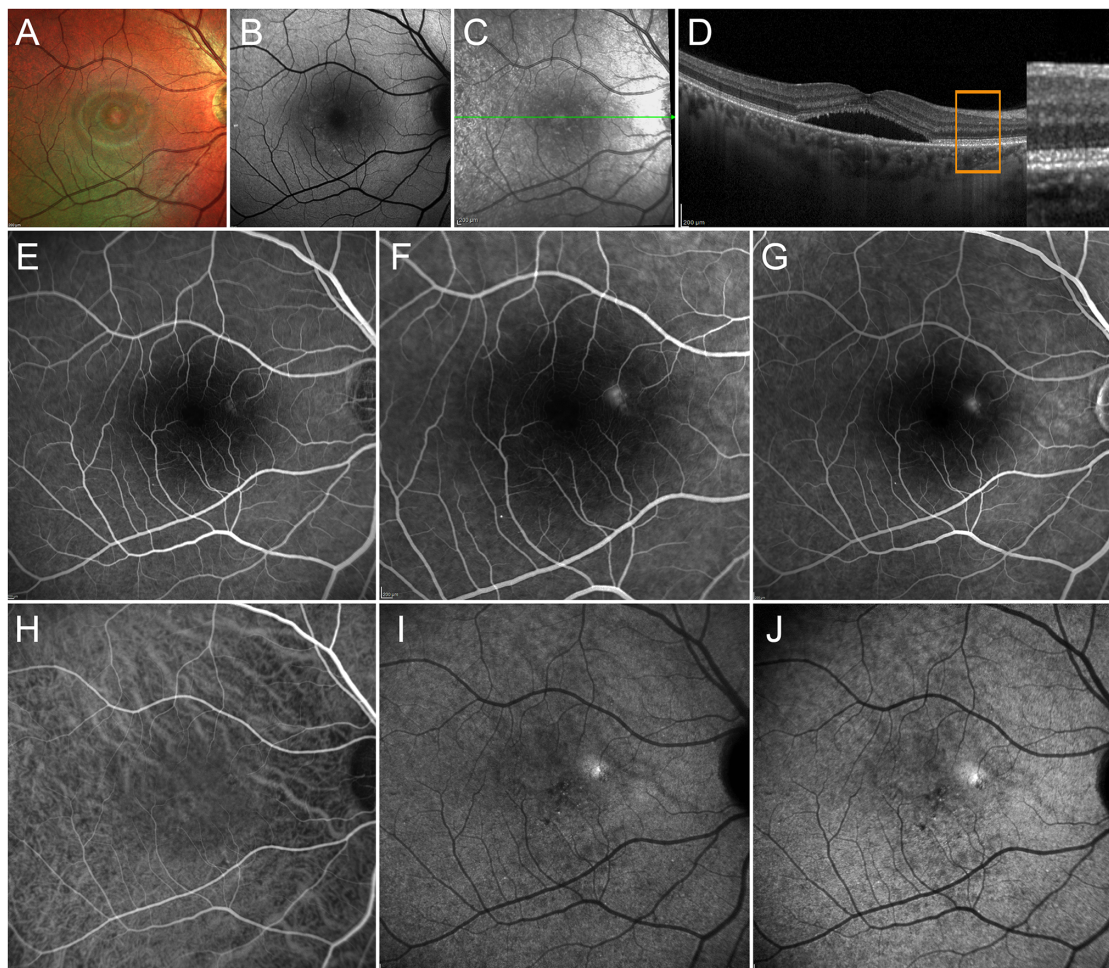
Figure 2. RPE-CSC on multicolor (A), BAF (B), IR (C), and structural OCT (D). Structural OCT reveals normal choroid, subretinal fluid, and outer retinal band attenuations (better visualized in the magnified box). A poorly defined leaking point is detectable on FA (E, F, G). ICGA (H, I, J) is characterized by absence of choroidal abnormalities and irregular hypofluorescence in the late phases.

210 eyes of 210 healthy subjects (mean age 52 ± 14 years; 170 males (81%)); LogMAR BCVA 0.0 ± 0.0).

Considering the CSC group as a whole, baseline BCVA was 0.18 ± 0.25 LogMAR, increasing to 0.13 ± 0.21 LogMAR after two years ($F = 109.61$; $P < 0.01$); baseline CMT was 337 ± 126 µm, improving to 244 ± 84 µm after two years ($F = 96.58$; $P < 0.01$). Overall, CT was 408 ± 99 µm in CSC patients, and 343 ± 79 µm in the controls ($F = 45.93$; $P < 0.001$). Interestingly, only HLT was significantly thicker in CSC patients (304 ± 83 µm), compared with the controls (243 ± 63 µm) ($F = 68.03$; $P < 0.01$).

Based on our healthy cohort of 210 eyes of 210 controls (mean age 48 ± 14 years; 125 males), we defined a pachychoroid as a choroid with a CT greater than 460 µm.

RPE-CSC was found in 48 eyes (50%) and was characterized by normal choroidal thickness, uneven leaking point on FA, which turned out to be more clearly detectable on ICGA, and irregular hypofluorescence in the late ICGA phases with corresponding outer retinal band signal attenuations on structural OCT (Fig. 2). SLT was 93 ± 33 µm at baseline, turning out to be 95 ± 23 µm at one-year follow-up and 88 ± 19 µm at two-year follow-up (all $P > 0.05$). HLT resulted 231 ± 42 µm at baseline, 230 ± 47 µm at one-year follow-up and 233 ± 33 µm at two-year follow-up (all $P > 0.05$). Mean BCVA changed from 0.23 ± 0.32 LogMAR to 0.19 ± 0.23 LogMAR after the first year, and to 0.21 ± 0.22 LogMAR at the end of the follow-up ($P > 0.05$).

Choroidal-CSC was identified in another 48 eyes (50%) and was characterized by a pachychoroid, a well-defined leaking point on FA and ICGA, choroidal vessel dilations in early ICGA phases, followed by isofluorescent background on late ICGA phases, and absence of outer retinal band defects (Fig. 3). SLT resulted 135 ± 25 µm at baseline, 127 ± 25 µm at
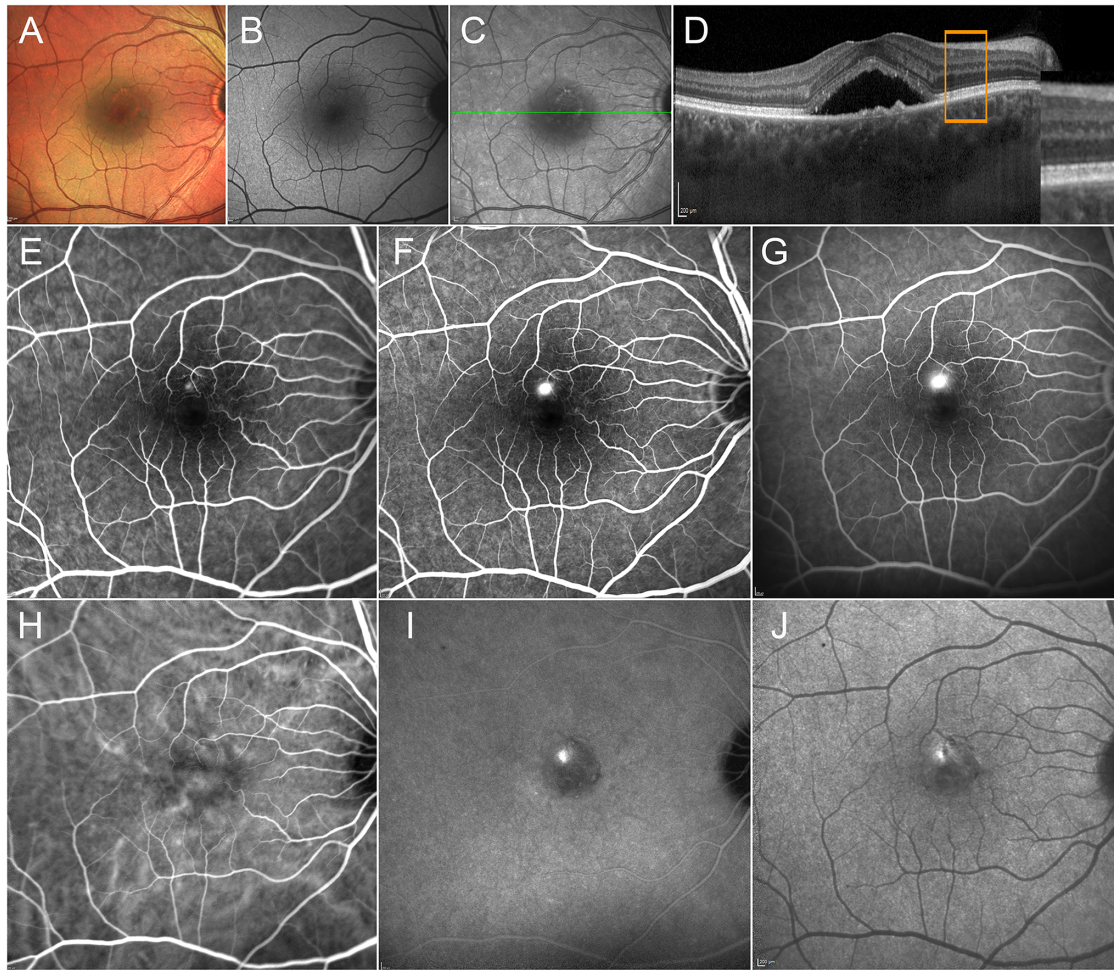
Figure 3. Choroidal-CSC on multicolor (A), BAF (B), IR (C), and structural OCT (D). Structural OCT shows pachychoroid and subretinal fluid, without outer retinal band alterations (shown in the magnified box). FA (E, F, G) reveals a well-defined leaking point. ICGA (H, I, J) reveals choroidal vessel alterations with isofluorescence in the late phases.

one-year follow-up, and 125 ± 22 µm at two-year follow-up ($P = 0.04$). HLT disclosed the following values: 358 ± 43 µm at baseline, 347 ± 50 µm at one-year follow-up, and 341 ± 56 µm at two-year follow-up ($P = 0.04$). Mean BCVA changed from 0.14 ± 0.12 LogMAR to 0.08 ± 0.25 LogMAR after the first year and 0.09 ± 0.16 LogMAR at the end of the follow-up ($P > 0.05$). The BCVA values proved significantly worse in RPE-CSC than in choroidal-CSC, considering baseline, one-year, and two-year follow-up values (all $P < 0.001$).

Overall, 18 eyes (19%) revealed MNV. In particular, 13 eyes (72%) were found in the RPE-CSC subgroup and five eyes (28%) in the choroidal-CSC subgroup ($P < 0.001$) (Table). A case of MNV is shown in Figure 4.

Forty out of 96 eyes (41%) were considered good responders to eplerenone 25 mg, whereas 38 eyes (40%) were switched to PDT. Good responders

to PDT required two $\pm$ one treatments over the whole follow-up. The MNV group of 18 eyes (19%) received a mean of seven $\pm$ three anti-VEGF injections over the 24-month follow-up. Eleven MNV eyes (60%) underwent additional PDT injections (three $\pm$ one sessions) to achieve a stabilized MNV with no fluid.

In the RPE-CSC subgroup without MNV, 20 eyes (57%) showed a good response to eplerenone, whereas 15 eyes (43%) were shifted to PDT showing a good response ($P > 0.05$). In contrast, 20 eyes (47%) in the choroidal-CSC subgroup were treated with eplerenone, achieving complete fluid resolution, while 23 eyes (53%) required PDT.

It is noteworthy that both SLT and HLT proved to be significantly thinner in RPE-CSC than in choroidal-CSC patients ($F = 78.57$; $P < 0.01$) during the whole follow-up. Remarkably, the MNV subgroup

Table. Clinical, Optical Coherence Tomography, and Optical Coherent Tomography Angiography Findings of Central Serous Chorioretinopathy Subgroups and Control Subjects

| | Quantitative Analyses in CSC Subgroups | | | |
	RPE-CSC Group	Choroidal-CSC Group	MNV Group	Controls
Group	1	2	3	4
Number of pts	35	43	18	210
LogMAR BCVA baseline	0.23 ± 0.32	0.14 ± 0.12	0.32 ± 0.18	0.0 ± 0.0
LogMAR BCVA 1-year F/U	0.19 ± 0.23	0.08 ± 0.25	0.25 ± 0.19	
LogMAR BCVA 2-year F/U	0.21 ± 0.22	0.06 ± 0.16	0.31 ± 0.26	
P value (2-Y vs. baseline)	0.09	0.02*	0.73	
CMT baseline (μm)	326 ± 139	374 ± 123	271 ± 66	233 ± 19
CMT 1-year F/U (μm)	245 ± 100	264 ± 84	228 ± 49	
CMT 2-year F/U (μm)	235 ± 76	253 ± 99	242 ± 57	
P value (2-Y vs. baseline)	<0.01*	<0.01*	0.07	
RT baseline (μm)	429 ± 91	463 ± 108	387 ± 94	347 ± 17
RT 1-year F/U (μm)	352 ± 76	361 ± 64	342 ± 56	
RT 2-year F/U (μm)	348 ± 61	362 ± 111	343 ± 86	
P value (2-Y vs. baseline)	<0.01*	<0.01*	0.07	
CT baseline (μm)	324 ± 36	493 ± 51	366 ± 107	340 ± 79
CT 1-year F/U (μm)	325 ± 48	473 ± 57	354 ± 125	
CT 2-year F/U (μm)	324 ± 39	466 ± 62	351 ± 133	
P value (2-Y vs. baseline)	0.99	<0.01*	0.09	
SLT baseline (μm)	93 ± 33	135 ± 25	49 ± 12	100 ± 21
SLT 1-year F/U (μm)	95 ± 23	127 ± 25	51 ± 11	
SLT 2-year F/U (μm)	88 ± 19	125 ± 22	42 ± 19	
P value (2-Y vs. baseline)	0.45	0.04*	0.14	
HLT baseline (μm)	231 ± 42	358 ± 43	317 ± 108	243 ± 63
HLT 1-year F/U (μm)	230 ± 47	347 ± 50	303 ± 125	
HLT 2-year F/U (μm)	233 ± 33	341 ± 56	309 ± 129	
P value (2-Y vs. baseline)	0.41	0.04*	0.31	
P Value	1 vs. 2	1 vs. 3	2 vs. 3	
BCVA baseline	0.63	0.14	0.007	
BCVA 2-year F/U	0.681	<0.01*	<0.01*	
CMT baseline (μm)	0.258	0.370	0.01*	
CMT 2-year F/U (μm)	>0.05	>0.05	>0.05	
RT baseline (μm)	0.407	0.448	0.023	
RT 2-year F/U (μm)	>0.05	>0.05	>0.05	
CT baseline (μm)	<0.01*	0.641	<0.01*	
CT 2-year F/U (μm)	<0.01*	0.628	<0.01*	
SLT baseline (μm)	<0.01*	<0.01*	<0.01*	
SLT 2-year F/U (μm)	<0.01*	<0.01*	<0.01*	
HLT baseline (μm)	<0.01*	<0.01*	0.06	
HLT 2-year F/U (μm)	<0.01*	<0.01*	0.333	

Legend: Statistically significant values are indicated by (*). The following abbreviations were used: best corrected visual acuity (BCVA), central macular thickness (CMT), retinal thickness (RT), choroidal thickness (CT), Sattler layer thickness (SLT), and Haller layer thickness (HLT).
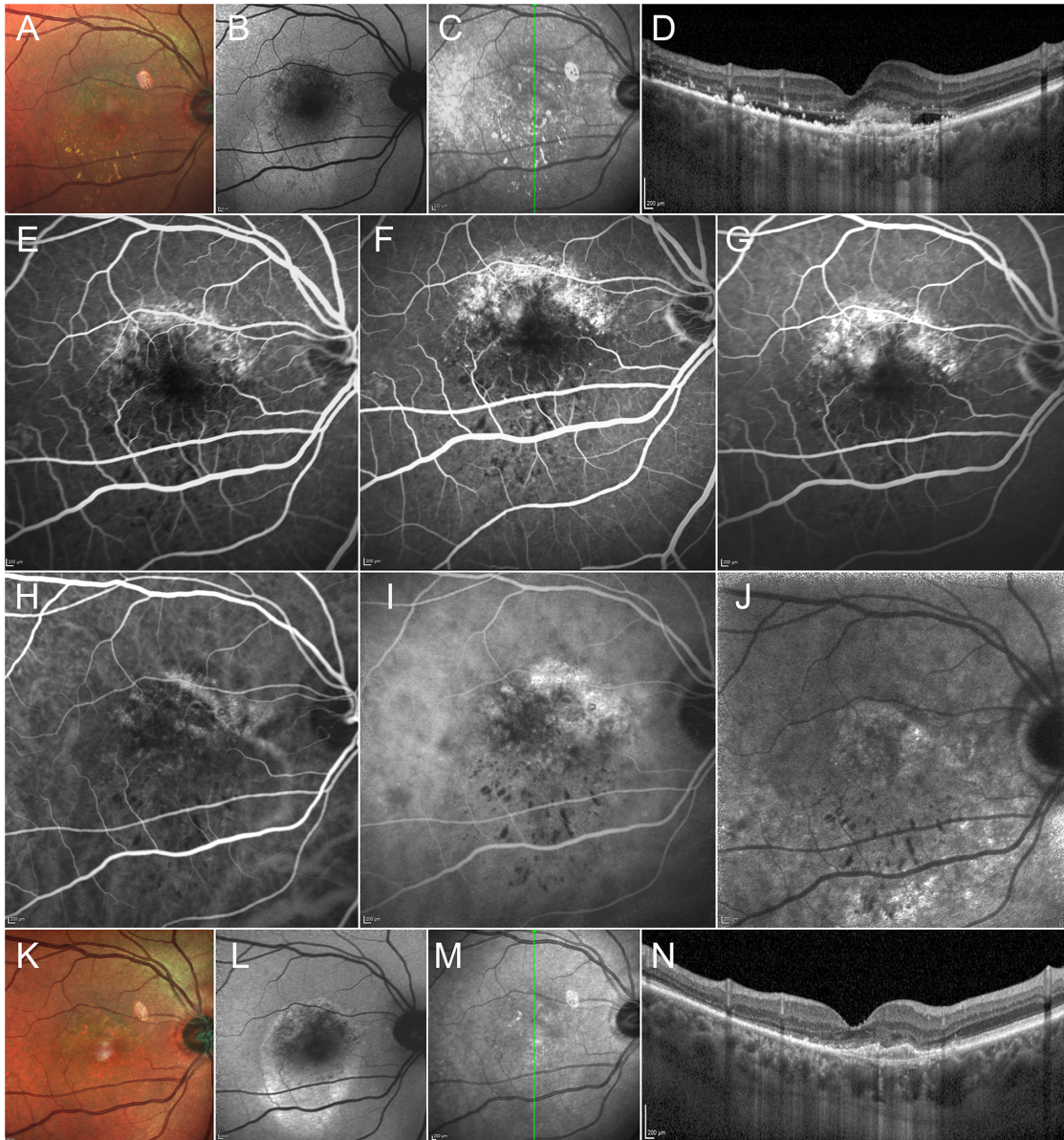
Figure 4. RPE-CSC complicated by MNV on multicolor (A), BAF (B), and IR (C). Structural OCT shows a choroid with normal appearance, subretinal fluid, and MNV. FA shows increased leakage from early to late stages (E, F, G). ICGA confirms the irregular late fluorescence at the posterior pole in addition to the MNV (H, I, J). Twenty-four months after ranibizumab treatment, a complete reabsorption of the fluid can be seen on multicolor, BAF, IR, and structural OCT images (K, L, M, N, respectively).

showed a further significant thinning of the Sattler layer, irrespective of whether the patients came from the RPE-CSC or the choroidal-CSC subgroups ($P < 0.01$) (Fig. 5). Furthermore, we registered a significant choroidal thinning only in the choroidal-CSC subgroup from baseline to the two-year follow-up. All the values are reported in the Table.

Overall, a pachychoroid was found in 20 eyes (50%) treated with eplerenone, in 18 eyes (47%) in the PDT subgroup, and in five eyes (28%) in the MNV subgroup.

Discussion

Multimodal imaging of CSC has revealed variable features, finding both RPE and choroidal alterations.[4–7] At the same time, we still lack a CSC classification correlating the disease phenotypes to the pathogenesis. Our study focused on identifying pachychoroid as the distinguishing feature differentiating two separate CSC subforms.
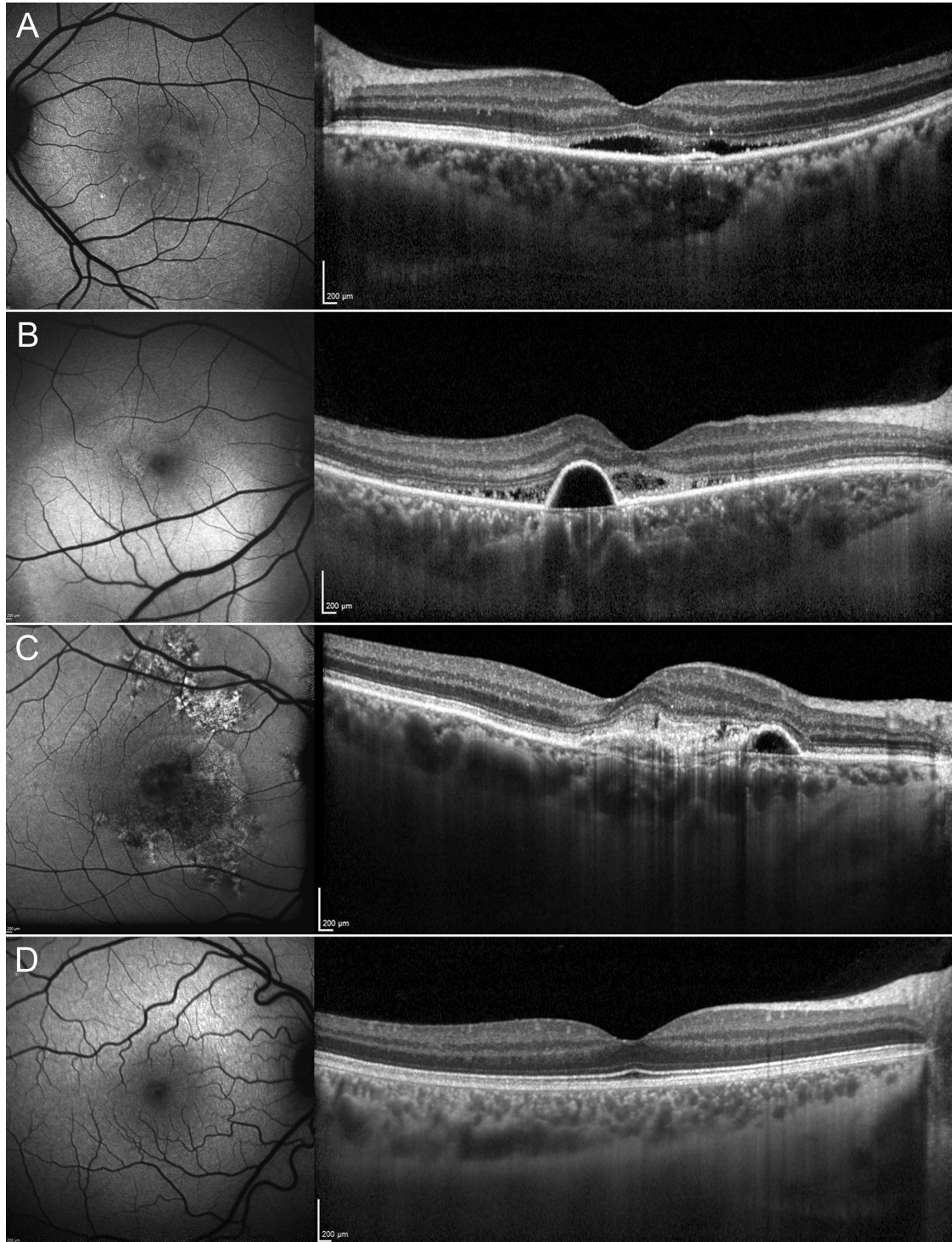
Figure 5. Sattler layer in CSC. RPE-CSC (mean SLT = 94 µm) (A) and choroidal-CSC (mean SLT = 98 µm) (B) showed a Sattler layer within normal limits. In contrast, MNV (C) showed a remarkably thin Sattler layer (mean SLT = 41 µm), compared with a healthy control (mean SLT = 102 µm) (D).

The absence of a pachychoroid characterized RPE-CSC, which typically showed a phenotype with normal choroidal thickness and irregular hypofluorescence in the late ICGA phases with corresponding outer retinal band signal attenuations on structural OCT. In contrast, the presence of a pachychoroid was typical of choroidal-CSC, which also displayed choroidal vessel dilation on early ICGA phases followed by

isofluorescent background on late ICGA phases, and absence of outer retinal band defects.

RPE-CSC recognizes the pathogenic influence of the RPE alterations, as evidenced by the combination of hypofluorescence on late ICGA and the corresponding finding of outer retinal band attenuations on structural OCT. The reduced indocyanine-green uptake of the RPE, resulting in irregular late hypofluorescence on ICGA, confirms the RPE impairment.[8,9]

Conversely, choroidal-CSC has a pathogenic key based on choroidal alterations, clinically expressed mainly as a pachychoroid on structural OCT, along with choroidal vessel dilation in early ICGA phases.

How a pachychoroid is defined is obviously crucial, but as yet there is no universally accepted quantitative metric defining a pachychoroid in the current literature. In our study, we decided to take the mean CT value of the control group and added it to double the standard deviation to identify the presence of a pachychoroid—only eyes with CT greater than 460 μm qualifying.

The apparently limited prevalence of pachychoroid in our series of eyes may be explained as the result of the strict cutoff we applied on the basis of a large sample of healthy control values.

Classifying the condition into RPE-CSC and choroidal-CSC subtypes had a direct clinical impact. First, the MNV complication turned out to be more frequent in RPE-CSC (72%) than in choroidal-CSC (28%). In addition, choroidal-CSC was associated with a better final visual outcome, compared with RPE-CSC (0.09 ± 0.16 vs. 0.21 ± 0.22 LogMAR in choroidal-CSC and RPE-CSC, respectively). This finding might be explained on one hand as reflecting the RPE involvement in the pathogenesis, with consequent dysfunction of the photoreceptors,[10] and on the other as expressing the greater prevalence of MNV. Moreover, eyes affected by RPE-CSC showed a slight tendency to respond to eplerenone better than choroidal-CSC, although further, more comprehensive studies are needed to provide a fuller evaluation of treatment responses in CSC.

Turning now to MNV, our data suggest that SLT thinning might represent a risk factor for the condition's onset, which may be favored by the impaired blood flow perfusion of the chorioretinal interface, with further RPE damage and increased release of cytokines and VEGF.[11]

We are aware that our study labors under a number of limitations. First, we have to underline that our inclusion criteria referred only to acute naive CSC cases, chronic CSC subforms being excluded ab initio. Moreover, since no patients were merely kept under observation but immediately treated, we cannot assert with confidence whether the final improvement

observed was secondary to eplerenone therapy or represented a spontaneous evolution. Throughout our research we bore in mind the recent study of Lotery and colleagues, which raised several doubts regarding the efficacy of eplerenone.[12] Even so, in view of previous investigations supporting a role of eplerenone in CSC,[13–17] we considered treatment with eplerenone to be a sensible first-line disease management strategy at the time when patients were recruited. Further studies are certainly warranted to determine whether a different patient stratification might justify a rationale for the use of eplerenone in CSC. It is also important to consider that all multimodal imaging techniques may have been affected by artifacts.

As regards the choroid assessment specifically, which was the crucial feature on which the RPE- and choroidal-CSC categorization hinged, we acknowledge that our definition of a pachychoroid may be considered arbitrary, even though it was based on a cutoff value drawn from a large sample of healthy subjects.

In conclusion, our study suggests that acute CSC includes two main clinical subtypes, displaying differing features as regards retina and choroid involvement, MNV development, and possibly response to treatments. Further data will need to be gathered to confirm our initial findings, extending the investigation to chronic CSC subforms.

Acknowledgments

References

1. Daruich A, Matet A, Dirani A, et al. Central serous chorioretinopathy: recent findings and new physiopathology hypothesis. *Prog Retin Eye Res*. 2015;48:82–118.

2. Iacono P, Battaglia Parodi M, Falcomatà B, Bandello F. Central serous chorioretinopathy treatments: a mini review. *Ophthalmic Res*. 2015;55(2):76–83.

3. van Rijssen TJ, van Dijk EHC, Yzer S, et al. Central serous chorioretinopathy: towards an

evidence-based treatment guideline. *Prog Retin Eye Res*. 2019;73:100770.

4. Cheung CMG, Lee WK, Koizumi H, Dansingani K, Lai TYY, Freund KB. Pachychoroid disease. *Eye (Lond)*. 2019;33(1):14–33.

5. Imamura Y, Fujiwara T, Spaide RF. Fundus autofluorescence and visual acuity in central serous chorioretinopathy. *Ophthalmology*. 2011;118(4):700–705.

6. Iacono P, Battaglia Parodi M, Papayannis A, La Spina C, Varano M, Bandello F. Acute central serous chorioretinopathy: a correlation study between fundus autofluorescence and spectral-domain OCT. *Graefes Arch Clin Exp Ophthalmol*. 2015;253(11):1889–1897.

7. Gattoussi S, Freund KB. Multimodal imaging in central serous chorioretinopathy. *Ophthalmology*. 2017;124(9):1331.

8. Chang AA, Morse LS, Handa JT, et al. Histologic localization of indocyanine green dye in aging primate and human ocular tissues with clinical angiographic correlation. *Ophthalmology*. 1998;105(6):1060–1068.

9. Gaudric A, Mrejen S. Why the dots are black only in the late phase of the indocyanine green angiography in multiple evanescent white dot syndrome. *Retin Cases Brief Rep*. 2017;11(Suppl 1):S81–S85.

10. Sparrow JR, Hicks D, Hamel CP. The retinal pigment epithelium in health and disease. *Curr Mol Med*. 2010;10(9):802–823.

11. Le YZ, Bai Y, Zhu M. Relationship between the RPE-produced VEGF and the outer blood-retina barrier function. *Invest Ophthalmol Vis Sci*. 2008;49(13):857.

12. Lotery A, Sivaprasad S, O'Connell A, et al. Eplerenone for chronic central serous chorioretinopathy in patients with active, previously untreated disease for more than 4 months (VICI): a randomised, double-blind, placebo-controlled trial. *Lancet*. 2020;395(10220):294–303.

13. Schwartz R, Habot-Wilner Z, Martinez MR, et al. Eplerenone for chronic central serous chorioretinopathy–a randomized controlled prospective study. *Acta Ophthalmol*. 2017;95(7):e610–e618.

14. Zucchiatti I, Sacconi R, Parravano MC, et al. Eplerenone versus observation in the treatment of acute central serous chorioretinopathy: a retrospective controlled study. *Ophthalmol Ther*. 2018;7(1):109–118.

15. Salehi M, Wenick AS, Law HA, Evans JR, Gehlbach P. Interventions for central serous chorioretinopathy: a network meta-analysis. *Cochrane Database Syst Rev*. 2015;(12):CD011841.

16. Leisser C, Hirnschall N, Hackl C, Plasenzotti P, Findl O. Eplerenone in patients with chronic recurring central serous chorioretinopathy. *Eur J Ophthalmol*. 2016;26(5):479–484.

17. Cakir B, Fischer F, Ehlken C, et al. Clinical experience with eplerenone to treat chronic central serous chorioretinopathy. *Graefes Arch Clin Exp Ophthalmol*. 2016;254(11):2151–2157.